Available online at www.sciencedirect.com
SCIENCE DIRECT®
Journal of Nuclear Materials 335 (2004) 311–321
journal of nuclear materials
www.elsevier.com/locate/jnucmat

Microstructural investigation of the stability under irradiation of oxide dispersion strengthened ferritic steels

I. Monnet [a,*], P. Dubuisson [a], Y. Serruys [b], M.O. Ruault [c], O. Kaïtasov [c], B. Jouffrey [d]

[a] CEA/DEN/SRMA, CEA Saclay, 91191 Gif sur Yvette cedex, France
[b] CEA/DEN/DMN/SRMP, CEA-Saclay, 91191 Gif sur Yvette cedex, France
[c] CSNSM, IN2P3/CNRS, bat 108, 91405 Orsay campus, France
[d] LMSS-Mat, Ecole centrale de Paris, 92295 Châtenay Malabry, France

Received 5 August 2003; accepted 6 May 2004

Abstract

Some fuel pin cladding made from a ferritic steel reinforced by titanium and yttrium oxides were irradiated in the French experimental reactor Phénix. Microstructural examination of this alloy indicates that oxides undergo dissolution under irradiation. This irradiation shows the influence of dose and, in a smaller part, of temperature. In order to better understand the mechanisms of dissolution, three ferritic steels reinforced by Y_2O_3 or MgO were irradiated with different charged particles. Inelastic interactions induced by 1 MeV He ion irradiation do not lead to any modification, neither in their chemical composition, nor in their spatial and size distribution. In contrast, isolated Frenkel pairs created by electron irradiation lead to significant oxide dissolution with a radius decrease proportional to the dose. Moreover, the comparison between irradiation with ions (displacements cascades) and electrons (Frenkel pairs only) shows the importance of free point defects in the dissolution phenomena.

PACS: 61.82.Bg; 61.16.Bg; 61.80.Fe; 61.80.Hg; 61.80.Jh

1. Introduction

Actual austenitic stainless steels are not suited for high temperature, high fluence (>80 dpa) nuclear applications because of their large swelling under irradiation. Oxide dispersion strengthened ferritic martensitic steels (ODS) are considered for these applications. ODS ferritic steels are highly resistant to swelling thanks to the cubic centred structure of the matrix. ODS alloys also offer improved out-of-pile strength characteristics at temperatures above 550 °C thanks to the fine oxide dispersion. An experimental irradiation in Phénix of a ferritic ODS type alloy, named DY (Fe–13Cr–1.5Mo + $1TiO_2 + 0.5Y_2O_3$) indicates that yttrium oxide undergoes dissolution under neutron irradiation [1,2]. For this type of materials, several kinds of phenomena can be responsible for such a dissolution (thermal dissolution, recoil dissolution, dissolution induced by displacement

* Corresponding author. CIRIL, CEA-CNRS-ENSICAEN, BP 5133, 14070 Caen cedex 5, France. Tel.: +33 231 45 46 70; fax: +33 231 45 47 14.
E-mail address: monnet@ganil.fr (I. Monnet).

0022-3115/$ - see front matter
doi:10.1016/j.jnucmat.2004.05.018

cascades, dissolution due to inelastic interaction, etc.). In order to improve the understanding of the mechanisms of dissolution, DY and two other ferritic steels (Fe–9Cr) reinforced by Y_2O_3 or MgO were irradiated with different sorts of charged particles.

2. Experimental procedure

2.1. Materials

The ODS ferritic steel named DY has been developed by CEN-SCK Mol (Belgium) [3,4]. It has been prepared by mechanical alloying from elementary metallic elements and Y_2O_3 and TiO_2 powders. Its chemical composition is given in Table 1. The last two heat treatments were a solution annealing at 1050 °C for 15 min and an ageing at 800 °C for 24 h. The microstructure is composed of two types of grains, elongated in the extrusion direction. The first type contains few dislocations (recrystallised grains) and the other shows a high tangled dislocation density (Fig. 1(a)). All grain boundaries are decorated by an intense precipitation of quaternary intermetallic χ phases ($Fe_{42}Cr_9Ti_5Mo_2$). Except for a few oxide-free bands parallel to the direction of extrusion, the oxide dispersion is homogeneous throughout the grains. No difference in oxide distribution has been observed between grains which are recrystallised or not. During the fabrication of these alloys, the chemical composition of the oxides has changed. Their chemical composition was determined by X-ray analysis on thin foil specimens. There are two oxide populations. A homogeneous dispersion of fine oxides (<50 nm) with a regular shape (Fig. 1(b)): these particles are yttrium oxide (85Y–10Al–<5Ti,O) or titanium–yttrium oxide (70Y–25Ti–10Al,O). There are also larger oxides (50 nm to 1 μm), some of them with a dendritic interface. There are also mixed titanium–yttrium oxides (70Y–25Ti–10Al,O) and titanium oxides (>90Ti,O).

The other materials, two EM10 (Fe–9Cr–1Mo) ferritic steels respectively reinforced by Y_2O_3 or MgO, were elaborated by mechanical alloying in a Netzsch PR01 attritor. Each mill was charged with 8 kg of 8 mm diameter 100C6 balls and 400 g of powder. The powders consist of 0.4% in volume of oxide powder (Y_2O_3 or MgO) and a powder of EM10 steel (Fe–9Cr–1Mo) produced by argon atomising process. The powder obtained after 80 h milling under argon is densified by coextrusion with

Table 1
The chemical composition of ODS ferritic steels (wt%)

Material	Fe	C	Cr	Mo	Mn	Si	Al	Ti	Mg	Y	O
DY	Balance	0.015	12.9	1.48	0.08	0.03	0.05	2.03	–	0.45	0.3
EM10 + Y_2O_3	Balance	0.010	8.6	1.15	0.51	0.38	–	–	–	0.18	0.13
EM10 + MgO	Balance	0.093	8.74	1.01	0.52	0.39	0.02	–	0.11	–	0.16

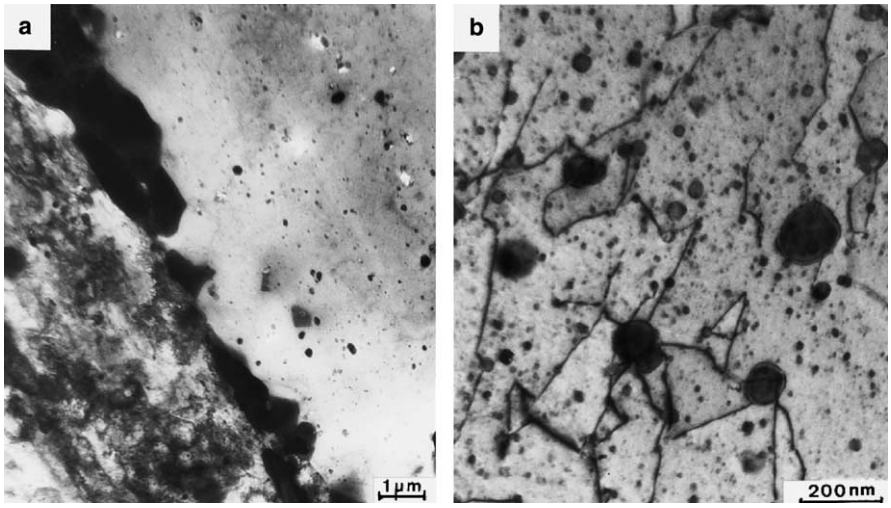

Fig. 1. Microstructure of the ODS ferritic steel DY before irradiation. (a) The two types of grains and χ phase. (b) Oxide distribution in a recrystallised grain.

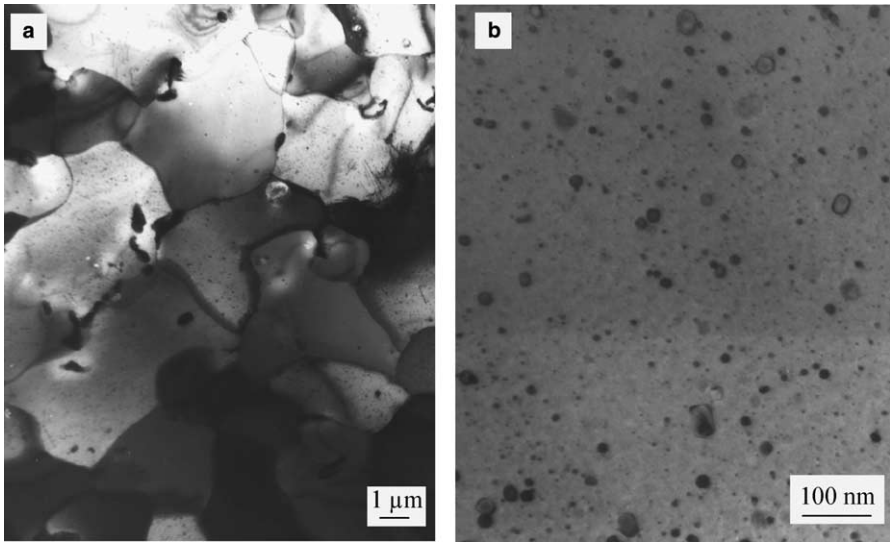

Fig. 2. Microstructure of EM10 steel reinforced by MgO before irradiation. (a) Isotropic grains, big oxides and carbides. (b) Fine and homogeneous oxide dispersion.

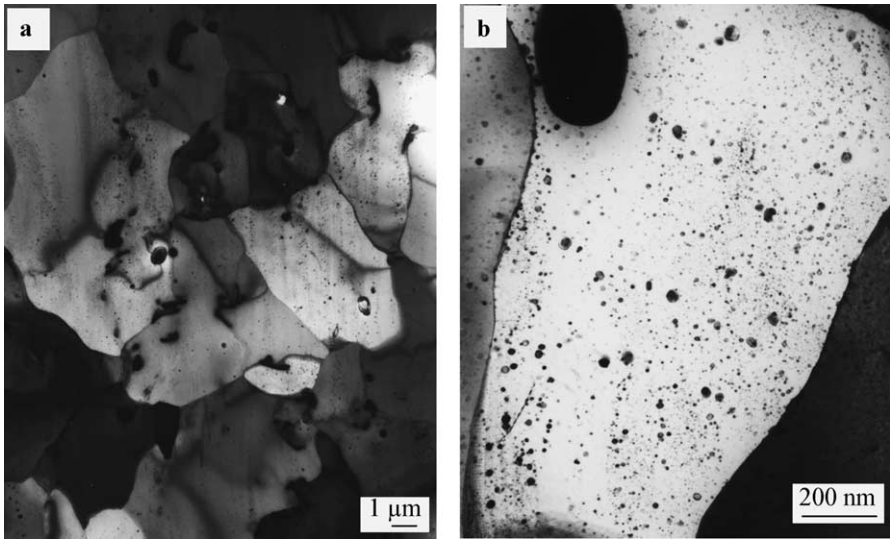

Fig. 3. Microstructure of EM10 steel reinforced by Y_2O_3 before irradiation. (a) Isotropic grains, big oxides and carbides. (b) Fine and homogeneous oxide dispersion.

mild steel clad [5]. The chemical composition of these specimens is shown in Table 1. In order to have a dislocation-free matrix, to see better the oxides, the materials were heated at 1100 °C for 30 min and then slowly cooled at 1 °C/min. These materials are made of small isotropic grains, containing complex carbides $M_{23}C_6$ (M = 30Fe–60Cr–10Mo) (Figs. 2(a) and 3(a)). Two populations of oxides coexist. There is first a family of big oxides (>50 nm). These big oxides are amorphous silicon oxides or specific oxides containing Mg or Y but also a large amount of manganese or silicon. Besides, there is also a population of small oxides (<50 nm). This fine dispersion is homogeneous, the average diameter is about 10 nm for EM10 + MgO and 15 nm for EM10 + Y_2O_3 (Fig. 2(a) and 3(b)). The chemical composition of the oxides has been modified during alloy elaboration. They now contain elements which were in solution in the EM10 powder before the fabrication. Table 2 indicates the different compositions of oxides discovered in these two materials.

Table 2
Oxide chemical composition

Material	Oxide	Y	Al	Mg	Mn	Si
EM10 + MgO	SiO_2					100
	MgO			50	15	35
	MgO			20	35	40
	$MgAl_2O_4$		65	20		15
EM10 + Y_2O_3	SiO_2					100
	Y_2O_3	85				15
	Y_2O_3	75			10	15

2.2. Observations

Specimens were mechanically thinned to 0.1 mm thickness. To make transmission electron microscopy discs, a TENUPOLE device was used with the 721 electrolyte at 13 °C and a current of 200 mA.

Before and after irradiation, TEM examinations have been performed on an EM 430 Philips electron microscope equipped with a LaB_6 filament and operating at 300 kV. To examine the change in composition caused by irradiation, scanning energy dispersive spectrometry (STEM/EDS) was used. It allows the study of the chemical composition of the matrix and the oxides by X-ray microanalysis before and after irradiation. To carry out these experiments, an electron probe diameter of about 7 nm was used.

2.3. Irradiation

2.3.1. Neutron irradiations

A few fuel pin claddings made from DY steel were irradiated in an experimental capsule placed in a special subassembly in the central part of the Phénix reactor core. The maximum dose reached was 81 dpa, and temperatures ranged from 400 to 580 °C along fuel pins. TEM examinations were performed on six locations of a fuel pin cladding. The locations and their irradiation conditions are given in Table 3. One of them serves as a reference for the non-irradiated state.

2.3.2. Electron irradiations

Electron irradiations and in situ observations were carried out in the high voltage electron microscope (HVEM) of C.E.A. Saclay using a beam of 1 or 1.2 MeV electrons. The irradiated areas were always in an orientation avoiding the contrast of the dislocation loops formed under irradiation in the ferritic matrix (out of contrast orientation). Irradiations were done with a focused beam of 2 μm diameter. The central beam intensity ranges from 1 to 2×10^{20} $e^-/cm^2/s$, which corresponds to 3 to 6×10^{-3} dpa/s in the ferritic matrix, assuming a displacement cross-section of 40 barns. Irradiations have been performed in the temperature range of 300–550 °C. The beam current is constant in its centre over 1 μm. Since the diameter of the oxides is 200–600 nm, a constant dose is thus kept constant on the oxide.

The evolution of the chosen oxide was followed during all the irradiation and micrographs were taken every 10 dpa in order to measure the oxide area with a planimeter. The foil was not tilted during the experiment to prevent the artefacts due to the not perfectly spherical shape of the oxide. The evolution of the diameter of the oxides with the dose was deduced from the evolution of the diameter of a sphere of the same diametral area as the oxide.

2.3.3. Ion irradiations

1MeV helium ions irradiations were done with a 1 MV Van de Graaf accelerator (SRMP, C.E.A. Saclay), at 400 °C. In order to avoid elastic interactions, we have observed only the first 200 nm of the irradiated zones (far from the implantation zone). To do this, we have irradiated 3 mm discs, electro-polished only on one face, and then we have observed thin foils by TEM, after electro-polishing the other face.

Irradiations using 300 keV argon ions were done with a 180 keV accelerator (IRMA, CSNSM-Orsay, France). This accelerator is coupled with a Philips transmission

Table 3
Location and irradiation conditions of TEM specimens

Location mm/BCF[a]	−400	105	285	375	465	850
Temperature (°C)	400	435	484	508	532	580
Dose (dpa)	≈0	54.8	75.6	79.3	78.8	30.5

[a] Bottom of column fuel.

Table 4
Microstructural evolution of the oxides distribution

Irradiation conditions	Disappearance of the small oxides	Halo of subparticles	Halo diameter (nm)	Chemical composition
400 °C, 0 dpa	No	No		3 families slight loss of Al
435 °C, 54 dpa	No	Extremely faint	<50	2 families loss of Al
450 °C, 62 dpa	No	Faint	40–60	2 families loss of Al
484 °C, 75.6 dpa	Yes	Large	80–100	2 families loss of Al
508 °C, 79.3 dpa	Yes	Large	80–100	2 families loss of Al
532 °C, 78.8 dpa	Yes	Large	90–110	2 families loss of Al
580 °C, 30.5 dpa	No	Faint	50	2 families loss of Al

electron microscope working at 120 kV, allowing in situ experiments. In situ observations have been performed at 400 °C, for a maximum dose reaching 33 dpa in the ferritic matrix.

3. Results

3.1. Neutron irradiations

In a previous paper, we described the behaviour of the ODS ferritic steel irradiated as fuel pin cladding in Phénix (DY). The main microstructural results are [1,2]:

- The general microstructure of DY does not appear to be modified during the in-pile service. Both types of elongated grains are still present and the chemical composition of the matrix is about the same, with only a little decrease of Cr content. Intergranular χ phases seem to be unaffected, however there is an increase of Cr and Mo content and a decrease of Ti content, correlated with irradiation temperature rather than with fluence.
- The strong ductility loss induced by the irradiation results from a fine and uniform α' precipitation and the dislocation loop formation at low temperature (as in classic ferritic steels) and from an intense χ phase precipitation at higher temperature (>450 °C).
- Another invocated cause of the embrittlement of this ODS ferritic steel under irradiation is the dissolution/reprecipitation of the oxides, leading to the disappearance of the homogeneous distribution of oxides and to the formation of a halo of smaller oxides around the larger ones. This heterogeneous distribution, with area without oxides coexisting with area where the density of very small oxides is high could make the materials more brittle.
- A few voids are observed at low temperature (<500 °C) leading to a swelling value close to zero. Voids are mainly associated with oxide particles.

In this paper we focus on the dissolution of the oxides. Microstructural observations indicate that the oxide evolution consists in four phenomena:

(i) The interfaces of the oxide particles with the matrix become irregular.
(ii) The uniform distribution of the finest oxides (<20 nm) disappears in high-dose irradiated specimens (>60 dpa).
(iii) A halo of fine oxides appears around the larger ones. The halo width increases with fluence.
(iv) The chemical composition of the oxides changes, even for specimens irradiated at low dose. The oxides lose more aluminium and titanium atoms than yttrium atoms.

Microstructural evolution of the oxides distribution is summarized in Table 4, for each irradiation condition.

At the bottom of the clad, where the dose is close to 0 dpa, the oxides seem to be unaffected by thermal ageing in the reactor. The chemical composition determined by X-ray microanalysis has slightly changed (slight decrease in aluminium content), but both the density and size of the oxides remain constant.

At higher fluence, the oxides are affected by in-pile irradiations. At 30.5, 54 and 62 dpa, the density of fine oxides seems to be similar to the density of fine oxides in unirradiated ODS, but there is a modification of larger ones. A halo of very small oxide particles surrounds the latter (Fig. 4(c)). Furthermore, the chemical composition has changed: the oxides have lost aluminium atoms and, in a smaller proportion, titanium atoms.

For the highest doses, close to 70–80 dpa, the uniform distribution of fine oxides seems to be less dense (Fig. 4(b)). The chemical composition of the oxides is the same as the chemical composition of the less irradiated oxides. In Fig. 5 the contents of the main metallic Y, Al and Ti elements of the oxides in the specimen irradiated at 532 °C, are plotted as a function of Fe content, which is the main element in the matrix and are compared to those obtained on the unirradiated alloy. This procedure allows for the separation of different oxides in spite of the matrix contribution when small particles are analysed in thin foils. After irradiation, titania and only one type of yttria are detected. All the oxides have lost their aluminium during in-pile service and yttria contains no more than 15% of titanium instead of 25% before irradiation. The oxides in all the other

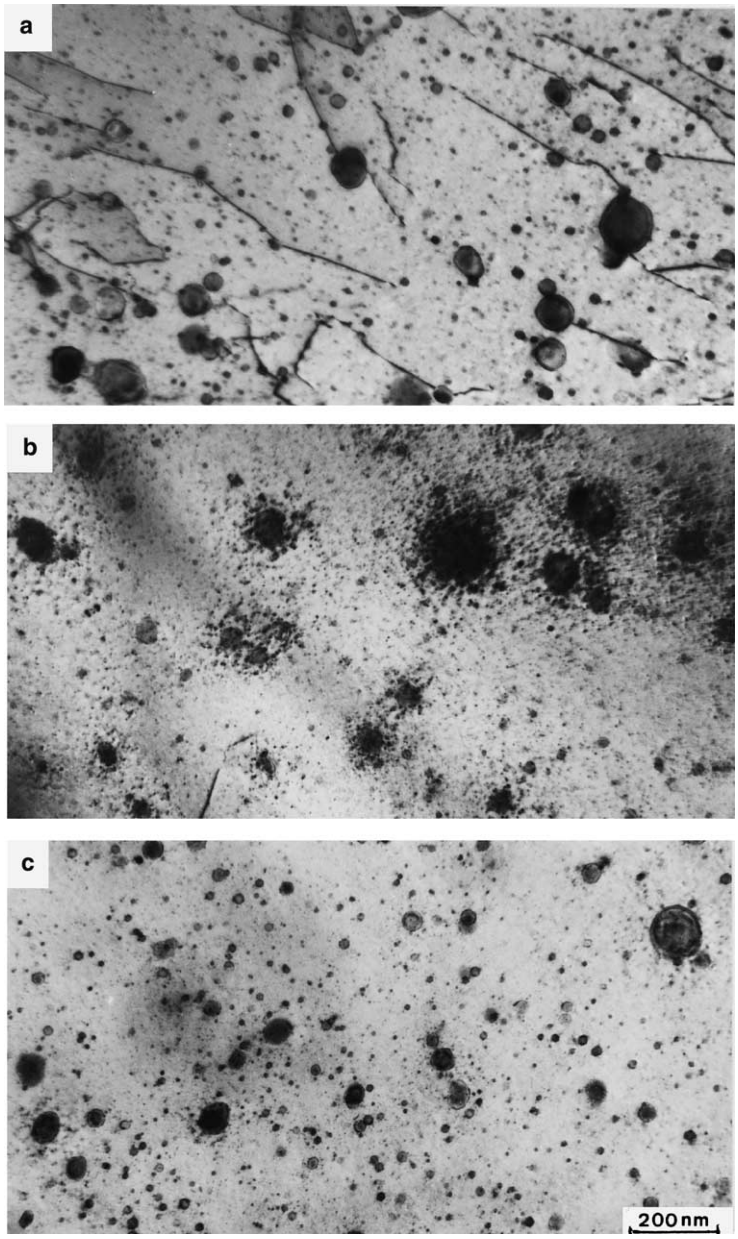

Fig. 4. Oxide dispersion in the DY ODS steel: (a) before irradiation, (b) after irradiation at 532 °C to 78.8 dpa and (c) after irradiation at 580 °C to 30.5 dpa.

irradiated specimens (from 30.5 to 79.3 dpa) present the same evolution. The halo of small oxides surrounding the biggest ones is more visible than in the specimens irradiated at 30.5 dpa (Fig. 4(b) and (c)). The tiny particles around the oxides contain Y, Ti and Al in the same proportions as the oxide they are surrounding (Fig. 5).

At the highest doses, we can see the influence of temperature since we dispose of three irradiated specimens at nearly the same doses (about 75 dpa) and at temperatures ranging from 474 to 532 °C. There is no influence of the temperature on the modification of the chemical composition and on the density of original oxides. The only influence is on the tiny particles composing the halos. The halos surrounding the biggest oxides become larger when the temperature increases and the size of the small particles composing the halo decrease.

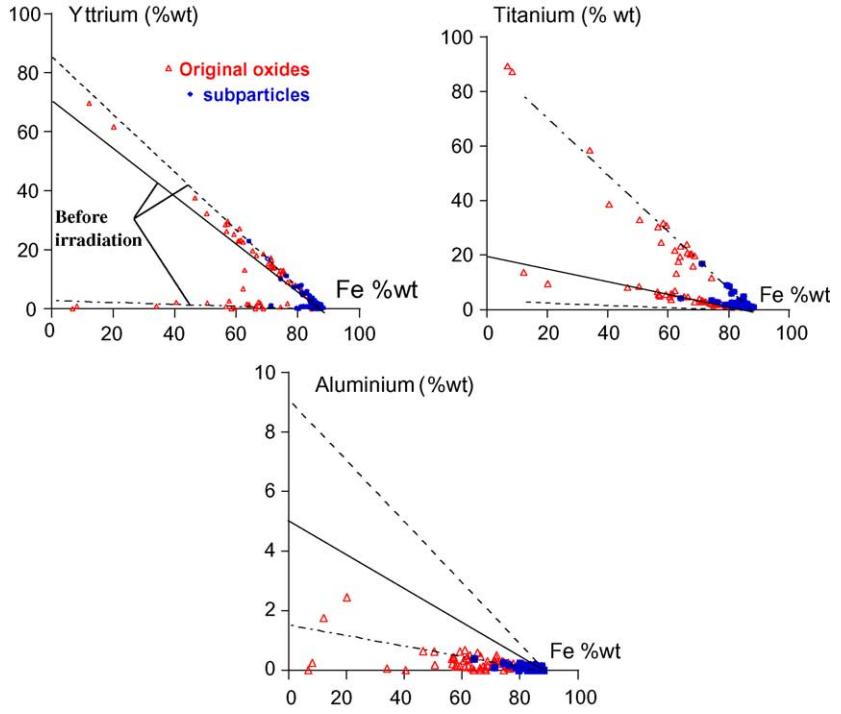

Fig. 5. X-ray microanalysis on thin foil of DY irradiated at 532 °C to 78.8 dpa (original oxides (△) and subparticles (♦)) – comparison with the three types of oxides present before irradiation [solid line, titanium–yttrium oxide (70Y–25Ti–10Al,O); dash line, yttrium oxide (85Y–10Al–<5Ti,O), and alternating dash line, titania (>90Ti,O)].

3.2. Helium irradiations

Fig. 6 compares the electronic stopping power and the nuclear stopping power of 1 MeV helium ions. Along the observed zone (the 200 first nanometers) the majority of energy is lost by electronic interaction (99.8%). Since the projected range of 1 MeV helium ion in Fe is 1.68 μm, there are very few implanted helium atoms in the observed area.

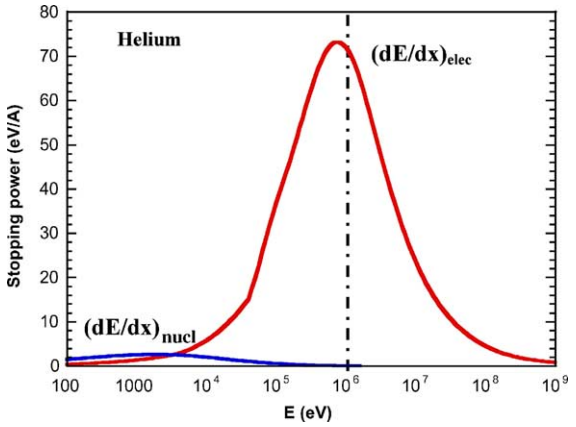

Fig. 6. Stopping power for helium ion in pure Fe.

The three materials, DY, EM10 + MgO and EM10 + Y_2O_3 were irradiated with 1 MeV helium ions at 400 °C with a total fluence of 1.6×10^{16} ions/cm^2. TRIM simulation indicates that the observed zones have received less than 0.05 dpa during the irradiation. Irradiation with 1 MeV helium ions does not induce any modification, neither in the chemical composition of the particles nor in their spatial and size distribution.

3.3. Electron irradiations

Fig. 7 shows the oxide size modification during in situ irradiation of an oxide of EM10 + MgO with 1 MeV electrons at 400 °C. The oxides of EM10 + MgO irradiated with 1 MeV electrons decrease in size. The decrease is more important when temperature increases, as shown on Fig. 8. The decrease in diameter is always proportional to the fluence, except for the highest temperature (550 °C). At 300 °C, we have performed irradiation on two oxides of different size (120 and 200 nm in diameter, respectively). Fig. 7 indicates that the radius loss do not depend on original size.

For both ODS steels reinforced by yttrium oxides (EM10 + Y_2O_3 and DY), the oxides do not show any

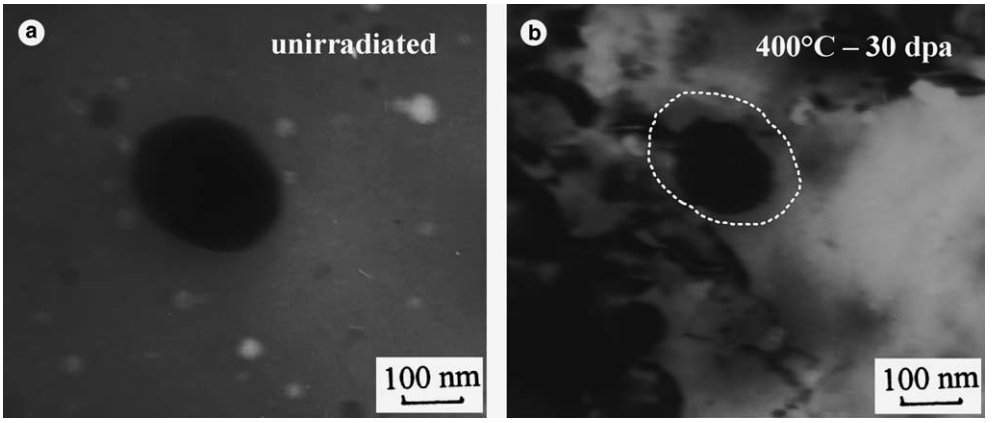

Fig. 7. Oxide evolution in EM10 + MgO irradiated with 1 MeV electron at 400 °C: (a) 0 dpa and (b) 30 dpa.

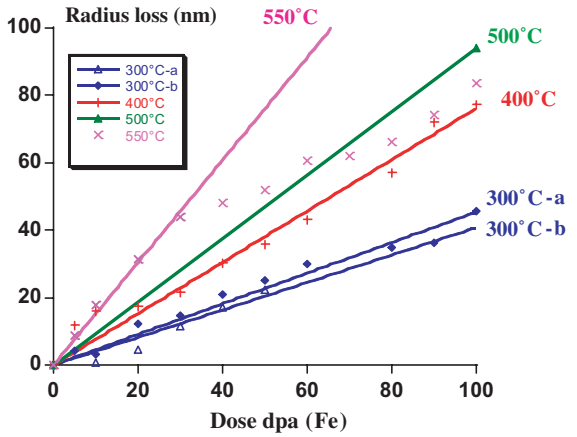

Fig. 8. Radius evolution of magnesium oxides during 1 MeV electron irradiation.

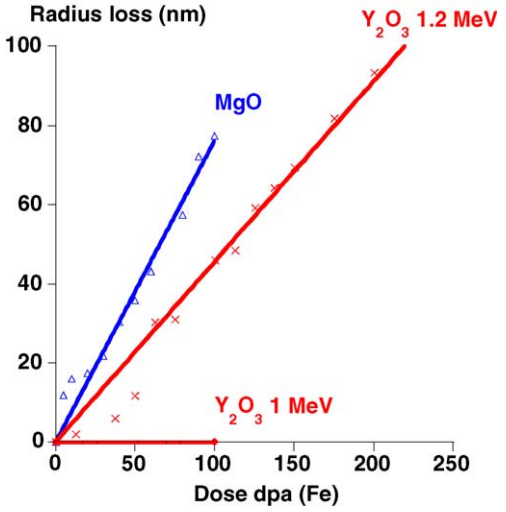

Fig. 9. Comparison between MgO irradiated with 1 MeV electrons and Y_2O_3 irradiated by 1 and 1.2 MeV electrons.

evolution under 1 MeV electron irradiation, neither in size, nor in chemical composition. But, under irradiation with 1.2 MeV electrons, the oxides decrease in size. The diameter shrinkage varies linearly with the fluence (Fig. 9). At equal dose yttrium oxides are less dissolved by 1.2 MeV electrons than magnesium oxides by 1 MeV electrons.

3.4. Argon irradiations

For the EM10 + MgO ferritic steel, an irradiation with 300 keV argon ions leads to a weak dissolution of the oxides. The diameter shrinkage is less than 5 nm after an irradiation at 400 °C up to 33 dpa. The shape of the oxides becomes more rounded (Fig. 10). During irradiation, the same matrix orientation has been kept in order to prevent artefacts due to oxides shape.

Alike EM10 + MgO, the oxides of EM10 + Y_2O_3 undergo a slight dissolution under irradiation with 300 keV argon ions. Furthermore, the yttrium oxides became amorphous.

4. Discussion

First we can notice that the dissolution of the oxides observed after in-pile irradiation can be reproduced by ion or electron irradiations. The only phenomenon that is not reproduced by such experiments is the formation of a halo of small oxides around the biggest ones. This is probably due to the fact that, for neutron irradiated specimens, the fuel pin has been kept during 600 h at a temperature higher than 400 °C after the irradiation. Yttrium, in solid solution in the ferritic matrix due to the dissolution of oxides, could then reprecipitate during

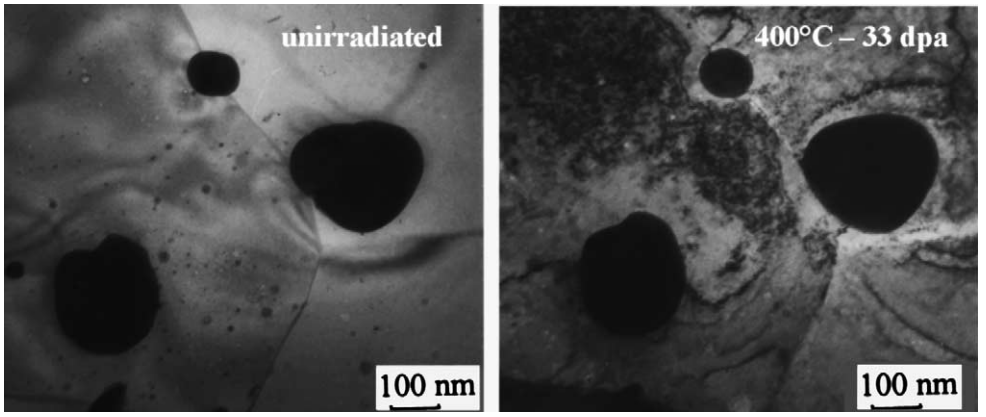

Fig. 10. Oxide evolution in EM10 + MgO irradiated with 300 keV argon ions at 400 °C.

this anneal (the solubility of yttrium in α-Fe is nearly zero at 400 °C). This kind of reprecipitation is not possible during ion or electron irradiations because of the rapid cooling after the irradiation.

The irradiation in Phénix reactor indicates that the yttrium oxides undergo dissolution under neutron irradiation. For this type of material, several kinds of phenomena can be responsible for such dissolution (thermal dissolution, recoil dissolution, dissolution induced by displacement cascades, dissolution due to inelastic interaction, etc.). The comparison between the different irradiations leads us to find some mechanisms which have an effect on oxide dissolution under irradiation:

(i) 1 MeV helium ion irradiations do not induce any modification of the oxides dispersion. Since in such thin samples most of the energy of helium ions is lost by inelastic interaction, these results prove that this kind of interaction does not induce oxide dissolution and cannot be responsible for the behaviour observed under neutron irradiation.

(ii) Electron irradiations lead to the dissolution of the oxides. These experiments prove that isolated Frenkel pairs can induce oxide dissolution and that the displacement cascades are not necessary. Electron irradiations give another important information about oxides dissolution since yttrium oxides are not affected by 1 MeV electron irradiations and undergo dissolution under 1.2 MeV electron irradiation: in fact, 1 MeV electrons do not have enough energy to displace yttrium atoms, whereas 1.2 MeV electrons have enough energy to displace Y (see Table 5). Hence, yttrium displacements appear to be necessary for Y_2O_3 dissolution to occur.

Irradiations with electrons lead to a significant dissolution with a radius decrease proportional to the dose, provided metallic atoms are displaced. To obtain oxide dissolution, it is necessary to displace both the metallic element and oxygen.

Table 5
The displacement threshold energy (E_d) for Y, Mg and O [6,7] and the maximum transferred energy (E_t) by 1 or 1.2 MeV electron

	E_d	E_t 1 MeV	E_t 1.2 MeV
Y in Y_2O_3	57	49	64
O in Y_2O_3	57	271	357
Mg in MgO	55	178	235
O in MgO	55	271	357

(iii) At the same fluence (33 dpa in the matrix) and at the same temperature (400 °C), the oxides of EM10 + MgO show a radius shrinkage of 5 nm under 300 keV argon irradiation and of 22 nm under 1 MeV electron irradiation. It is well-known that only a fraction of displaced atoms in cascade cores survives after the first stages of the collision process. Assuming that in our ions irradiations only one-third of the displaced atoms survive as free point defects [8], an irradiation up to 33 dpa with argon corresponds to an irradiation up to 10 dpa with 1 MeV electrons, for which all the defects are Frenkel pairs. For an irradiation at 400 °C with 1 MeV electrons up to 10 dpa, the radius shrinkage of an oxide of EM10 + MgO is about 7 nm, as for an irradiation up to 33 dpa with argon ions (about 5 nm). This indicates that the free defects induce the dissolution. The disorder induced by the displacement cascades has a small influence. Nevertheless, this disorder seems to have an effect on the amorphisation of the yttrium oxides, since they become amorphous under ion irradiations but not under electron irradiations, for similar damage rate and temperature.

(iv) Nelson et al. [9] and Frost and Russel [10] have modelled the phenomenon of particle dissolution by ballistic mechanisms: the atoms of the oxides have been put in solution during the collisional process directly in the surrounding matrix. We propose a simple model, based

Table 6
Comparison between calculated and experimental decrease of diameter for magnesium oxides irradiated with 1 MeV electrons

T (°C)	Fluence (dpa for matrix)	E_t max (eV) O/Mg	R (nm) O/Mg	$\phi_{initial}$ (nm)	Estimate ϕ_{final} (nm)	Experimental ϕ_{final} (nm)
300	50	271/178	8/6	700	696	660
300	100	271/178	8/6	450	444	358
400	100	271/178	8/6	546	537	390
500	100	271/178	8/6	628	621	440

on these earlier models, in order to estimate the diameter shrinkage of the oxides undergoing ballistic dissolution. We have not taken care of back-diffusion, hence the diameter shrinkage is overestimated.

This simplistic model will permit a determination of whether only ballistic dissolution occurs or other mechanisms must be taken into account.

The rate at which solute atoms enter the matrix is the rate at which there are recoils created in the oxide and expelled into the matrix. This can be described as a source generation term $G(r)$ in the matrix, which depends on the radius r from the oxide centre. All recoils are assumed to travel a particular distance R, and to occur randomly in all directions. The source term is given by Gelles and Garner [11] as

$$G(r) = \frac{S}{4rR}\left(r_p^2 - (r-R)^2\right) \quad \text{for } r_p < r < R \text{ and } R < 2r_p, \tag{1}$$

with S the volumetric recoil generation rate and r_p the radius of the oxide.

Integration of Eq. (1) allows us to determine the redeposition rate N:

$$N = \int_{r_p}^{r_{p+R}} 4\pi r^2 G(r)\,\mathrm{d}r = \frac{\pi S}{R}\left(r_p^2 R^2 - \frac{R^4}{12}\right). \tag{2}$$

Assuming that the loss of volume of the oxide corresponds to the volume of ejected atoms, the decrease of diameter of the oxide during dt is

$$\mathrm{d}r = \frac{-r_p K}{3}\left(\frac{3R}{4r_p} - \frac{R^3}{16r_p^3}\right)\mathrm{d}t, \tag{3}$$

where $K = Sv_{at}$ is the atomic displacement rate, and for $R > 2rp$

$$\mathrm{d}r = \frac{-r_p K}{3}\,\mathrm{d}t.$$

Then, the evolution of the oxide radius can be determined

$$\begin{cases} r(0) = r_p, \\ r(t+\Delta t) = r(t) + \Delta r. \end{cases}$$

Table 6 compares the experimental final radius and the calculated final radius for 1 MeV electron irradiations of the oxides of EM10 + MgO ferritic steel. The distance R is estimated with TRIM considering the length of recoil of oxygen or magnesium atoms which received an energy equal to the maximum energy transmitted by the electron (E_t) in a simulation with 1.2 MeV krypton ions (using complete cascade description).

This method over-estimates the decrease of diameter since we did not take care of back-diffusion: we considered that the loss of volume is equal to the volume of ejected atoms and we supposed that the transferred energy is the maximum one. Nevertheless, the experimental decrease is far more important than the calculated one. The ballistic dissolution is not sufficient to explain such an important diameter shrinkage under electron irradiations.

Ultimately, it is necessary to take into account the creation of point defects and their diffusion inside the oxides leading to the diffusion of oxide elements (oxygen and metallic atoms) in the surrounding matrix to explain the dissolution. This is confirmed by the effect of temperature on this phenomenon, showing the importance of diffusion process.

5. Conclusion

A clad made with an ODS ferritic steel, called DY (Fe–13Cr–1.5Mo + TiO_2 + Y_2O_3) has been irradiated in the French experimental Phénix reactor. Seven transmission electron microscopy discs were taken along the fissile column in order to improve the understanding of the influence of temperature and dose in the microstructural evolution of this material. The matrix evolution is in agreement with the evolution of 9–14 Cr ferritic steels under irradiation in the same conditions. A new phenomenon under irradiation, the dissolution of the oxides, is observed. Microstructural observations indicate that oxide evolution consists in four phenomena:

- The interfaces of oxide particles with the matrix become irregular.
- The uniform distribution of the finest oxide (<20 nm) disappears in the highly irradiated specimen (>60 dpa).
- A halo of fine oxides appears around the larger oxides. The halo width is proportional to fluence.

- The chemical composition of oxides changes, even for low-dose irradiated specimens. The oxides lost their aluminium and more titanium than yttrium.

There is no evolution of oxide dispersion for the specimen irradiated at 400 °C up to less than 1 dpa, showing that the oxide dissolution observed in the other specimens irradiated at different temperatures with doses greater than 30.5 dpa is due to irradiation and not to thermal ageing. No temperature dependence of oxide evolution is observed, except for the width of the halo for specimens irradiated at high doses, which increases with temperature.

Irradiation with neutrons shows the influence of dose and, less significantly, of temperature. But this kind of irradiation does not allow us to distinguish the influence of inelastic interaction, Frenkel pairs or displacement cascades formation because all these types of phenomena are present. In order to improve the understanding of the mechanisms of dissolution, DY and others ferritic steels (Fe–9Cr) reinforced by Y_2O_3 or MgO were irradiated with different charged particles:

- Irradiation with 1 MeV helium does not induce any modification, neither in the chemical composition of the particles nor in their spatial and size distribution. Since in such thin samples most of the energy of helium ions is lost by inelastic interaction, this result proves that this kind of interaction does not induce oxide dissolution.
- Irradiation with electrons leads to a significant dissolution of oxides with a radius decrease proportional to the dose. These experiments prove that Frenkel pairs can induce oxide dissolution.
- The comparison between irradiation with ions (displacements cascades) and electrons (Frenkel pairs only) shows the importance of free point defects in the dissolution phenomena.
- A simple model shows that ballistic ejection of atoms alone cannot be responsible for the observed loss of diameter of oxide particles. Hence, the role of point defects diffusion has to be taken into account, which is in agreement with the existence of an effect of temperature.

Acknowledgments

The authors would like to thank X. Averty (CEA-DEN/DMN/SEMI) for the neutron irradiated thin foil preparation and D. Simeone for fruitful discussions.

References

[1] P. Dubuisson, R. Schill, M.P. Hugon, I. Grislin, J.L. Seran, in: R.K. Nanstad, M.L. Hamilton, F.A. Garner, A.S. Kumar (Eds.), Effects of Radiation in Materials: 18th International Symposium, ASTM STP 1325, American Society for Testing and Materials, West Conshohocken, PA, 1999, p. 882.
[2] I. Monnet, PhD thesis, Report CEA-R-5868 (1998).
[3] J.J. Huet, L. Coheur, L. De Wilde, J. Gedopt, W. Hendrix, W. Vandermeulen, in: J.W. Davis, D.J. Michel (Eds.), Proceedings of the Topical Conference on Ferritic Alloys for use in Nuclear Energy Technologies, The Metallurgical Society, Warrendale, PA, USA, 1984, p. 329.
[4] L. De Wilde, J. Gedopt, S. De Burbure, A. Delbrassine, C. Driesen, B. Kazimierzak, in: Materials for Nuclear Reactor Core Applications, vol. 2, Proceedings of the International Conference, Bristol, UK, 27–29 October 1987, British Nuclear Energy Society, London, UK, 1987, p. 271.
[5] R. Baccino, A. Alamo, V. Lambard, F. Moret, in: Conference Euromat 96, Bournemouth, UK, 21–23 October 1996, Institute of Materials, UK, 1996, p. 551.
[6] M.D. Rechtin, H. Wiedersich, Radiat. Eff. 31 (1977) 181.
[7] S.J. Zinkle, C. Kinoshita, J. Nucl. Mater. 251 (1997) 200.
[8] R. Vascon, N.V. Doan, in: 17th International Conference on Atomic Collisions in Solids (ICACS-17), Beijing, China, 2–6 July 1997, Nucl. Instrum. and Meth. B 135 (1–4) (1998) 207.
[9] R.S. Nelson, J.A. Hudson, D.J. Mazey, J. Nucl. Mater. 44 (1972) 318.
[10] H.J. Frost, K.C. Russel, J. Nucl. Mater. 103&104 (1981) 1427.
[11] D.S. Gelles, F.A. Garner, J. Nucl. Mater. 85&86 (1979) 689.